Quadriwave lateral shearing interferometry for quantitative phase microscopy of living cells

Pierre Bon[1,2,*]. Guillaume Maucort[1,2]. Benoit Wattellier[2] and Serge Monneret[1]

[1]*Aix-Marseille Université, Ecole Centrale Marseille, CNRS, Institut Fresnel, Campus de Saint-Jérôme, 13013 Marseille, France.*

[2]*PHASICS SA, XTEC Bat. 404, Campus de l'Ecole Polytechnique, Route de Saclay, 91128 Palaiseau, France.*

pierre.bon@fresnel.fr

Abstract: Phase imaging with a high-resolution wavefront sensor is considered. This is based on a quadriwave lateral shearing interferometer mounted on a non-modified transmission white-light microscope. The measurement technology is explained both in the scope of wave optics and geometrical optics in order to discuss its implementation on a conventional microscope. In particular we consider the effect of a non spatially coherent source on the phase-image signal-to-noise ratio. Precise measurements of the phase-shift introduced by microscopic beads or giant unilamellar vesicles validate the principle and show the accuracy of the methods. Diffraction limited images of living COS-7 cells are then presented, with a particular focus on the membrane and organelle dynamics.

OCIS codes: (180.3170) Interference microscopy. (170.3880) Medical and biological imaging. (120.5050) Phase measurement. (290.3030) Index measurements.

References and links

1. F. Zernike, "Das Phasenkontrastverfahren bei der mikroskopischen Beobachtung", *Z. Tech. Phys.* **16**, 454–457 (1935).
2. G. Nomarski, "Nouveau Dispositif Pour l'Observation En Contraste De Phase Differentiel", *J. Phys. Radium* **16**, S88–S88 (1955).
3. P. Hariharan, "Achromatic Phase-Shifting for White-Light Interferometry", *Appl. Opt.* **35(34)**, 6823-6824 (1996).
4. C. J. Cogswell, N. I. Smith, K. G. Larkin and P. Hariharan, "Quantitative DIC microscopy using a geometric phase shifter", *Society of Photo-Optical Instrumentation Engineers (SPIE) Conference Series*, C. J. Cogswell, J. A. Conchello and T. Wilson, eds. (1997), pp. 72–81.
5. Y. Xu, Y. x. Xu, M. Hui and X. Cai, , "Quantitative surface topography determination by differential interference contrast microscopy", *Optics and Precision Engineering* **9**, 226-229 (2001).
6. M. R. Arnison, K. G. Larkin, C. J. R. Sheppard, N. I. Smith, and C. J. Cogswell, , "Linear phase imaging using differential interference contrast microscopy", *Journal of Microscopy* **214(1)**, 7–12 (2004).
7. S. Bernet, A. Jesacher, S. Fürhapter, C. Maurer and M. Ritsch-Marte, , "Quantitative imaging of complex samples by spiral phase contrast microscopy", Opt. Express **14(9)**, 3792–3805 (2006).
8. E. Cuche, F. Bevilacqua and C. Depeursinge, "Digital holography for quantitative phase-contrast imaging", *Opt. Lett.* **24(5)**, 291–293 (1999).
9. P. Marquet, B. Rappaz, P. J. Magistretti, E. Cuche, Y. Emery, T. Colomb and C. Depeursinge, "Digital holographic microscopy: a noninvasive contrastimaging technique allowing quantitative visualization ofliving cells with subwavelength axial accuracy", *Opt. Lett.* **30(5)**, 468–470 (2005).
10. F. Charrière, A. Marian, F. Montfort, J. Kuehn, T. Colomb, E. Cuche, P. Marquet and C. Depeursinge, "Cell refractive index tomography by digital holographic microscopy", *Opt. Lett.* **31(2)**, 178–180 (2006).

#110519 - $15.00 USD Received 24 Apr 2009; revised 3 Jul 2009; accepted 6 Jul 2009; published 16 Jul 2009

11. W. Choi, C. Fang-Yen, K. Badizadegan, S. Oh, N. Lue, R. R. Dasari and M. S. Feld, "Tomographic phase microscopy", *Nature Methods* **4**, 717–719 (2007).
12. M. Born and E. Wolf, *Principles of Optics*, Cambridge University Press (1999).
13. J. Zou, A. Sautivet, J. Fils, L. Martin, K. Abdeli, C. Sauteret and B. Wattellier, "Optimization of the dynamic wavefront control of a pulsed kilojoule/nanosecond-petawatt laser facility", *Appl. Opt.* **47(5)**, 704–710 (2008).
14. R. V. Shack and B. C. Platt, "Production and use of a lenticular Hartmann screen", *J. Opt. Soc. Am.* **61**, 656 (1971).
15. A. Barty, K. A. Nugent, D. Paganin and A. Roberts, "Quantitative optical phase microscopy", *Opt. Lett.* **23(11)**, 817–819 (1998).
16. C. J. Bellair, C. L. Curl, B. E. Allman, P. J. Harris, A. Roberts and L. M. D. Delbridge, "Quantitative phase amplitude microscopy IV: imaging thick specimens", *Journal of microscopy* **214(1)**, 62-68 (2004).
17. C. Curl, C. J. Bellair, P. J. Harris, B. E. Allman, A. Roberts, K. A. Nugent and L. M. D. Delbridge, "Single cell volume measurement by Quantitative Phase Microscopy (QPM): A case study of Erythrocyte Morphology", *Cellular Physiology and Biochemistry* **17**, 193–200 (2006).
18. J. Primot and L. Sogno, "Achromatic three-wave (or more) lateral shearing interferometer", J. Opt. Soc. Am. A **12(12)**, 2679 (1995).
19. J. Primot, "Theoretical description of Shack-Hartmann wave-front sensor", *Optics Communications* **222**, 81-92 (2003).
20. J. Primot and N. Guérineau, "Extended Hartmann Test Based on the Pseudoguiding Property of a Hartmann Mask Completed by a Phase Chessboard", *Appl. Opt.* **39(31)**, 5715–5720 (2000).
21. S. Velghe, J. Primot, N. Guérineau, R. Haidar, S. Demoustier, M. Cohen and B. Wattellier, "Advanced wave-front sensing by quadri-wave lateral shearing interferometry", *Proc. SPIE* (2006).
22. M. J. Weber, *Handbook of Optical materials*, CRC Press (2003).
23. M. Angelova, S. Soléau, P. Méléard and P. Bothorel, "Preparation of giant vesicles by external AC electric fields. Kinetics and applications" in *Trends in Colloid and Interface Science V*, Steinkopff Darmstadt, eds., (1992), pp. 127–131.
24. J. F. Nagle and S. Tristram-Nagle, "Structure of lipid bilayers", *Biochim. Biophys. Acta* **1469(3)**, 159–195 (2000).
25. C. S. Chong and C. Colbow, "Light scattering and turbidity measurements on lipid vesicles", *Biochim. Biophys. Acta* **436**, 260–282 (1976).
26. F. C. Jensen, J. Anthony, R. V. G. Girardi and H. Koprowski (1964), "INFECTION OF HUMAN AND SIMIAN TISSUE CULTURES WITH ROUS SARCOMA VIRUS", *PNAS* **52(1)**, 53–59 (1964).
27. A. Sergé, N. Bertaux, H. Rigneault and D. Marguet, "Dynamic multiple-target tracing to probe spatiotemporal cartography of cell membranes", *Nature Methods* **5**, 687–695 (2008).

1. Introduction

One of the most important problems for biologists when concerned by microscopy is the poor amplitude contrast of most of the biological specimens. As a consequence, biologists often employ phase-contrast optical techniques that rely on an optical mechanism to transform minute refractive index variations in the specimen into corresponding amplitude changes in its actual image. The major advantage of such techniques is that living cells can be examined in their natural state without previously being killed, fixed and/or stained. Zernike contrast [1] permits a visualization of sample interfaces but with a relatively poor lateral resolution and the apparition of artifacts preventing any correct quantitative phase measurement.

Nomarski contrast (or DIC for Differential Interference Contrast) microscopy is a much more popular phase imaging technique that gives the sample phase gradient in one direction [2]. Images present an output intensity that is a mix of amplitude and phase gradient contrast with a non-linear response to optical path length gradient in the specimen. Standard DIC systems are mostly qualitative in nature. That is why several research projects proposed to apply phase-shifting methods to DIC to acquire linear phase gradient images [3] [4] [5]. In particular, a method combining phase shifting, two directions of shear and Fourier-space integration using a modified spiral phase have been proposed to extend the DIC microscopy to a quantitative linear phase imaging technique [6]. More recently, Bernet and coworkers [7] demonstrated that a sequence of at least 3 spatially filtered images, which were recorded with different rotational orientations of a spiral phase plate, could be used to obtain a quantitative reconstruction of both amplitude and phase information of a complex microscopic sample. For practical imaging, this

#110519 - $15.00 USD Received 24 Apr 2009; revised 3 Jul 2009; accepted 6 Jul 2009; published 16 Jul 2009

method requires to be calibrated with a reference phase sample.

Interferometry, and especially digital holography is of course also available to render phase structures visible with a microscope [8]. Digital holographic microscopy provides quantitative measurement of the optical path length distribution that allows living cells to be described with a diffraction-limited transverse resolution and a sub-wavelength axial accuracy [9]. More recently, this method was applied to perform optical diffraction tomography of a pollen grain [10], and tomographic imaging of cells and multicellular organisms [11]. Because they rely on a Mach-Zender interferometer, these methods require a temporally coherent source (usually a laser), and above all a reference arm of which the optical path length has to be carefully controlled.

Wavefront sensing is a well known technology for studying the aberrations of a light-beam. In most applications, only the lower-order aberrations (like spherical aberration or coma) are considered, because the lower the aberration order is, the stronger is the effect on the beam [12] [13]. As a consequence, a few thousands of phase measurement points are sufficient to analyze the beam wavefront and subsequently compensate low order aberrations, as allowed by Shack-Hartmann wavefront sensors (SHWFS) [14], mostly used in adaptive optics. The main function of a wavefront sensor (WFS) is to sample the phase in a given plane that generally corresponds to the plane where the sensor is placed : no need to use a reference arm, unlike digital holography. It is of course possible to optically conjugate the WFS plane with a given object plane. For phase microscopy, the phase-shift introduced by a sample placed in the object plane could be directly measured by the WFS, allowing quantitative phase-shift imaging where the WFS resolution and the measurement point number now become a key element that currently excludes the use of Shack-Hartmann sensors, that give limited resolution.

Digital wavefront sensing (DWFS) has been proposed that relies on observing the manner in which intensity images change with small defocuses and using these intensity changes to recover the phase [15]. Initially proposed under the Born approximation, the method has been extended on structurally simple thick objects symmetrical around the mid plan [16], and applied to measure the volume of erythrocytes under a range of osmotic conditions [17]. This technique needs multiple measurements (at least 3) in different shifted planes and the shift values need to be precise in order to obtain quantitative measurements.

In this paper, we propose a new application in phase-imaging microscopy for WFS based on quadri-wave lateral shearing interferometry (QWLSI) [18]. This technique requires only one measurement, without any mobile element, in order to recover the phase and intensity, unlike DWFS. QWLSI has the potential to sample intensity and phase images with a higher lateral resolution compared to Shack-Hartmann WFS [19]. Moreover, it is an achromatic interferometric technique compatible with the white-light illumination pathway of conventional wide-field microscopes. We consider the use of QWLSI combined with a conventional white-light transmission microscope. Although the properties of QWLSI using a Modified Hartmann Mask (MHM) have been rigorously studied by Primot et al. [20] we propose a simple link between wave optics and geometrical optics in order to explain the influence of the spatial coherence of the light source on the phase measurement. After a theoretical analysis of the QWLSI-based WFS, we demonstrate its interest for phase microscopy, and quantify its accuracy by measuring calibrated test samples. The technique is then applied to living cell imaging.

2. QWLSI interferogram formation and analysis

The electromagnetic field in the microscope image plane is measured using a quadri-wave lateral shearing interferometer (SID4-HR, Phasics SA, Palaiseau, France), directly plugged onto a lateral video port of an inverted microscope (TE2000-U, Nikon, Japan). Figure 1 shows the experimental configuration.

#110519 - $15.00 USD Received 24 Apr 2009; revised 3 Jul 2009; accepted 6 Jul 2009; published 16 Jul 2009

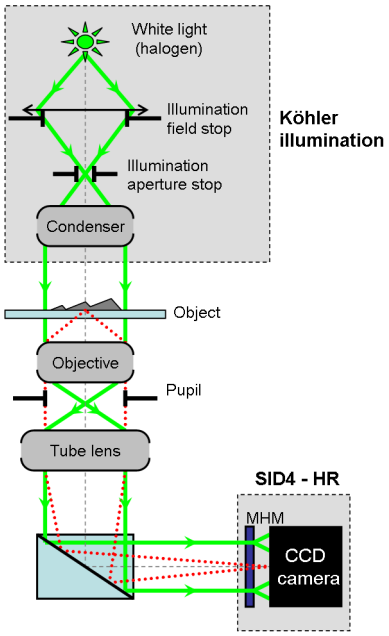

Fig. 1. Schematic layout of the setup.

Lateral shearing interferometry is a well-known technique to measure the phase gradients in one direction. The incident wave front is replicated into two identical but tilted wave fronts. After propagation, their mutual interference pattern is recorded with a CCD camera. The phase gradients are recovered from the fringe deformation, by means of a Fourier deconvolution around the interferogram fringe frequency. However, at this point, it lacks some gradient information to recover a full two dimensional phase-field. Multiwave interferometry [18] extends this principle to more than one gradient direction. In the case of QWLSI, four replicas are created by a specific 2D diffraction grating. In this case, two gradients along two perpendicular directions are measured and then integrated to determine the field intensity and phase [20].

The interferogram deformation can be interpreted using either the wave or geometrical optics. Wave optics is more rigorous and underlies the interferogram numerical processing. Whereas geometrical optics is more intuitive to understand physical effects, such as the influence of spatial coherence on interferogram contrast.

2.1. Interferogram formation

The incident light field complex amplitude is given in the frame of the slowly varying envelope by:

$$A(\mathbf{r}) = \sqrt{I(\mathbf{r})}\exp(i[\mathbf{k}\cdot\mathbf{r} - \varphi(\mathbf{r})]) \tag{1}$$

where $\mathbf{r}$ is the position vector, $\mathbf{k}$ the mean wave vector, I the field intensity, and φ the field phase. In the case of biological object observation, we are more interested in the modification of the Optical Path Difference (OPD) due to the presence of cell components. The phase and the OPD are simply linked by:

$$\varphi(\mathbf{r}) = \frac{2\pi}{\lambda}\mathrm{OPD} + \varphi(\mathbf{r}_0) \tag{2}$$

#110519 - $15.00 USD Received 24 Apr 2009; revised 3 Jul 2009; accepted 6 Jul 2009; published 16 Jul 2009

where r_0 is a reference vector.

A diffraction grating replicates the incident beam. In the case of our QWLS interferometer, the so-called Modified Hartmann Mask (MHM) is used [20]. It is made of the superposition of a Hartmann mask (amplitude grating of period p) and a π-shift checker board (phase grating of period $2 \cdot p$) as presented in the figure 2. This has been optimized to diffract more than 90% of the light energy into the 4 first orders carried by 4 wave vectors (see figure 2).

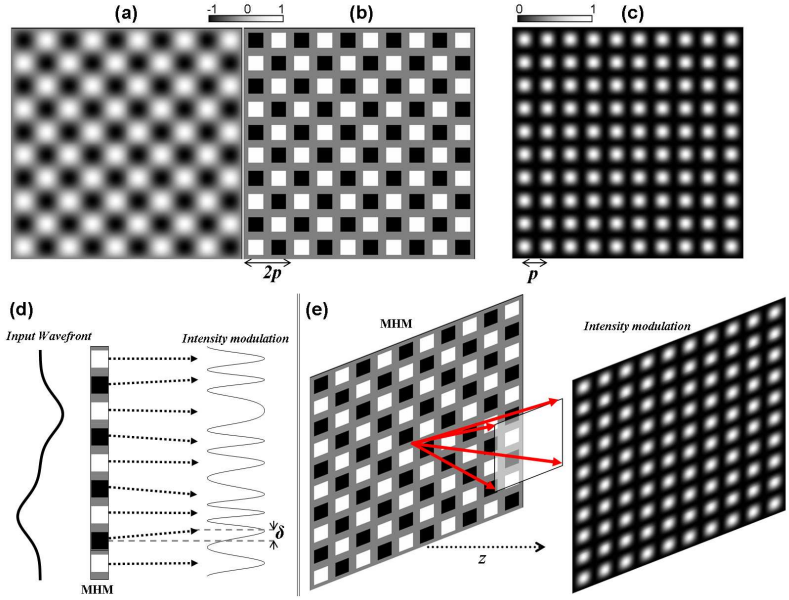

Fig. 2. (a) Ideal transparency for a 4-wave-only 2D diffraction grating. (b) MHM transparency, approximation of (a). (c) Intensity transmission of (a). (d) 1D interferogram formation by a MHM in the case of a disturbed input wavefront; geometrical approach. (e) 2D interferogram formation by a MHM in the case of a plane input wavefront; visualization of the 4 diffracted waves (arrows).

The amplitude transmittance of the perfect MHM, if only the 4 first orders are considered, is given by:

$$t(x,y) = \cos\left(\frac{\pi x}{p}\right) \cdot \cos\left(\frac{\pi y}{p}\right) \tag{3}$$

The corresponding intensity transmittance is:

$$\begin{aligned} T(x,y) &= |t(x,y)|^2 \\ &= \frac{1}{4}\left\{1 + \left[\cos\left(\frac{2\pi}{p}x\right) + \cos\left(\frac{2\pi}{p}y\right)\right] + \frac{1}{2}\left[\cos\left(\frac{2\pi}{p}(x+y)\right) + \cos\left(\frac{2\pi}{p}(x-y)\right)\right]\right\} \end{aligned} \tag{4}$$

Each diffracted order propagates along its own wave vector direction. After a propagation length z along the z-axis, in the scope of paraxial propagation and if we neglect free space diffraction, the electromagnetic field is the coherent addition of all the replicas, which are mutually displaced due to their deviation. It has already been shown, in a somewhat different form [21], that the intensity is given by :

#110519 - $15.00 USD Received 24 Apr 2009; revised 3 Jul 2009; accepted 6 Jul 2009; published 16 Jul 2009

$$I(\mathbf{r},z) = I_0\left\{1+\left[\cos\left(\frac{2\pi}{p}x+\frac{2\pi}{p}z\frac{\partial \mathrm{OPD}}{\partial x}\right)+\cos\left(\frac{2\pi}{p}y+\frac{2\pi}{p}z\frac{\partial \mathrm{OPD}}{\partial y}\right)\right]\right.$$
$$\left.+\frac{1}{2}\left[\cos\left(\frac{2\pi}{p}(x+y)+\frac{2\pi}{p}z\frac{\partial \mathrm{OPD}}{\partial (x+y)}\right)+\cos\left(\frac{2\pi}{p}(x-y)+\frac{2\pi}{p}z\frac{\partial \mathrm{OPD}}{\partial (x-y)}\right)\right]\right\} \quad (5)$$

where I_0 is the interferogram maximum of intensity in $z = 0$.

The interferometer sensitivity is determined by the ratio p/z. This means that the interferometer sensitivity is easily tunable by moving the grating back or forth in front of the CCD sensor. The same WFS can be used, for example, to study dense tissues or cells with little phase contrast.

The MHM can also be considered as a grid of holes and the classical interpretation of Hartmann and Shack-Hartmann wave front sensors [14] can be used. The incident wave front is sampled by the Hartmann holes. We record the projection of the holes in the CCD plane. Due to the local wave front slope, the projections deviate from their original position for a flat wave front by an amount δ (as shown in the figure 2):

$$\delta = -z \cdot \nabla \mathrm{OPD} \quad (6)$$

where z is the distance between the MHM and the CCD plane, and ∇ represent the vectorial gradient operator.

It is possible to calculate the intensity in the CCD plane as the intensity transmission at the points $\mathbf{r}-\delta$. The intensity in the CCD plane is deduced from equation 4, if we substitute (x,y) by $\left(x' = x+z\frac{\partial \mathrm{OPD}}{\partial x}, y' = y+z\frac{\partial \mathrm{OPD}}{\partial y}\right)$. It is straightforward to see that we obtain the same expression for the intensity as in equation 5. It is equivalent to use ray tracing or wave optics to deduce the intensity distribution. This property will be used later in the part 3.1 to study the interferogram contrast with extended sources. This equivalence has been thoroughly demonstrated for (Shack)-Hartmann WFS by Primot et al. [19].

2.2. Interferogram analysis

The interferogram is interpreted as a non-uniform OPD function, frequency-modulating a perfect sinusoidal pattern. The OPD gradients are then recovered by demodulating the recorded interferogram around its specific carrier frequencies. The result is two gradient fields, which are then integrated (see figure 3):

$$\begin{pmatrix} H_x \\ H_y \end{pmatrix} = \frac{2\pi}{p} z \begin{pmatrix} \frac{\partial \mathrm{OPD}}{\partial x} \\ \frac{\partial \mathrm{OPD}}{\partial y} \end{pmatrix} \quad (7)$$

From equations 5 and 7, both the interferogram period and the modulation due to the OPD are wavelength independent. The use of a temporally incoherent source (as a halogen lamp) is possible. Under the hypothesis of a wavelength independent sample OPD, the measured OPD with the WFS is the same using either a monochromatic source or a polychromatic one.

As a consequence, one can recover the OPD gradients from the Fourier analysis of the interferograms. The gradients are finally integrated to obtain a two dimensional OPD map. Because the phase information is coded in the interferogram by a frequency modulation, the phase and the intensity are independently determined. The intensity image is recovered by applying a low pass filter on the interferogram. This property is a great advantage over conventional phase contrast methods, such as Nomarski/DIC [2] or Zernike contrast [1], where it is very hard to attribute intensity modulations to either tissue absorption or OPD gradients.

#110519 - $15.00 USD Received 24 Apr 2009; revised 3 Jul 2009; accepted 6 Jul 2009; published 16 Jul 2009

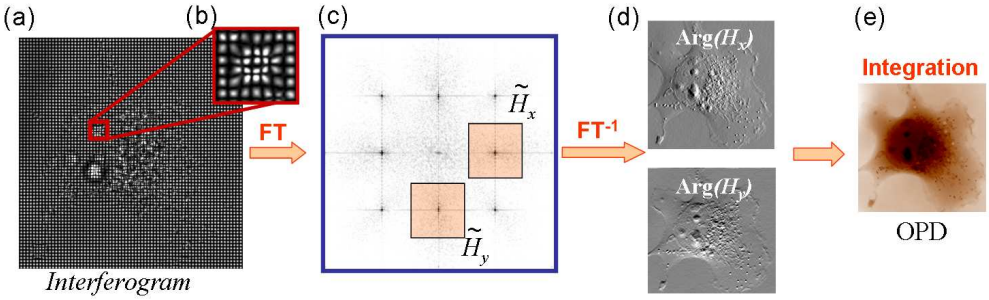

Fig. 3. (a) Interferogram obtained with an aberrant wavefront. (b) Zoom on a part of (a), visualization of the local frequency modulations. (c) Fourier Transform of (a). (d) Obtaining of 2 OPD orthogonal gradients by Inverse Fourier Transform of 2 sub-images of (b). (e) 2D Integration of the gradients to reconstruct the OPD.

The price for this is a reduction of the image resolution. For instance, in the present experiments, the intensity and phase images have a resolution 4 times smaller than the original recorded image. In this case the lateral sampling of intensity and phase is equal to $p \times p$ (the amplitude grating pitch, figure 2), and corresponds to 4×4 pixels on the CCD. It could be possible to optimize the interferogram sampling up to 2.73×2.73 pixels (Nyquist criterion).

3. Influence of the illumination on QWLSI phase imaging

As for any wavefront splitter interferometer, the interferogram contrast depends on the spatial coherence of the source. If the source is spatially incoherent, the measured interferogram is the sum of the interferograms formed by each elementary point of the illumination. The first effect is an interferogram contrast decrease. The second effect is a superposition of each different optical path within our sample, under different illumination angles. This second effect is more important with thick samples.

First we will propose a model of interferogram formation under partial spatially coherent illumination: this model is experimentally validated in the part 5.1. Then we will study the influence of the illumination numerical aperture on the signal-to-noise ratio (*SNR*) of an OPD measurement. The OPD superposition will be mentioned but the complete study goes beyond the scope of this paper.

3.1. Interferogram contrast

3.1.1. Theoretical point of view

Most of the wide-field microscopes use a Köler illumination system, where the aperture angle of the illumination determines the source spatial coherence. As the microscope is an afocal optical system, the maximum illumination angle θ_i in the image space is connected to the maximum illumination angle θ_o in the object space by the relation $\tan\theta_i = \tan\theta_o \cdot \frac{1}{g_y}$, where g_y is the lateral magnification of the microscope.

In order to modelize the microscope and the light source, we will study the effect of a collimated source, with tunable spatial coherence, on the interferogram contrast. In the case of an incoherent illumination, interferograms are summed incoherently and the intensity I is described by (8), considering the geometrical optics approach. The figure 4 shows the principle.

$$I(x,y) = \iint_S \mathrm{d}^2 I(x,y,x_s,y_s) \tag{8}$$

#110519 - $15.00 USD Received 24 Apr 2009; revised 3 Jul 2009; accepted 6 Jul 2009; published 16 Jul 2009

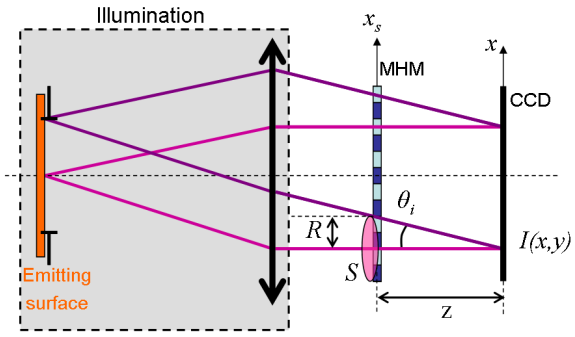

Fig. 4. Principle of the interferogram formation in case of an incoherent illumination.

where S is the equivalent emitting surface at the MHM plane and d^2I is the interferogram intensity formed by an elementary point of the emitting source. In the lambertian case, d^2I can be written as :

$$\mathrm{d}^2I(x,y,x_s,y_s) = \frac{I_{ponc}(x+x_s,y+y_s)}{S} \cdot \mathrm{d}x_s\mathrm{d}y_s \tag{9}$$

I_{ponct} is obtained by the formula (5) strongly simplified in the case of a plane incident wavefront :

$$I_{ponct}(x,y) = I_0 \cdot \left[1+\cos(Kx)+\cos(Ky)+\frac{1}{2}\cos\left(\sqrt{2}K\frac{x+y}{\sqrt{2}}\right)+\frac{1}{2}\cos\left(\sqrt{2}K\frac{x-y}{\sqrt{2}}\right)\right] \tag{10}$$

where $K = \frac{2\pi}{p}$ and p is the pitch of the MHM.

Assuming that the source is circular, the radius R of S is $R = z \cdot \frac{\tan(\theta_o)}{g_y} = z \cdot \tan(\theta_i)$ where z is the distance between MHM and CCD. (x_s,y_s) satisfies $\sqrt{x_s^2+y_s^2} \leq R$.

Relation (8) can be written in the polar coordinate system :

$$I(x,y) = \int_{\phi_s=0}^{2\pi}\int_{r_s=0}^{R} \frac{I_{ponct}(x+r_s\cdot\cos(\phi_s), y+r_s\cdot\sin(\phi_s))}{\pi R^2} \cdot r_s\,\mathrm{d}r_s\,\mathrm{d}\phi_s \tag{11}$$

By solving this integration, the interferogram intensity can be described by :

$$I(x,y) = I_0 \cdot \left[1+M(KR)\left[\cos(Kx)+\cos(Ky)\right]+\frac{1}{2}M\left(\sqrt{2}KR\right)\left[\cos(K\,[x+y])+\cos(K\,[x-y])\right]\right] \tag{12}$$

where M is equal to :

$$M(X) = \frac{2\cdot J_1(X)}{X} \tag{13}$$

The important fact here is that the modulation only depends on the pitch of the MHM grating and on the magnification of the microscope. It is also interesting to note that if the microscope is not perfectly afocal, there is no visible effect on the interferogram contrast. Indeed, in this case, the equivalent source radius R is modified and becomes :

#110519 - $15.00 USD Received 24 Apr 2009; revised 3 Jul 2009; accepted 6 Jul 2009; published 16 Jul 2009

$$R(D) = z \cdot \frac{\tan(\theta_o)}{g_y} \times \frac{1}{1 - z \cdot D / f_{TL}^2} = R_{afocal} \times \frac{1}{1 - z \cdot D / f_{TL}^2} \tag{14}$$

where D is the distance between the image focal plane of the objective and the object focal plane of the tube lens ($D = 0$ in the afocal case) ; f_{TL} is the focal length of the tube lens.

In general, $f_{TL} \approx 200mm$, $z \approx 1.5mm$; that means that if a 5% variation of R between the afocal and non afocal configuration is acceptable, D can vary from $0 \leq D < 1.25m$. In consequence, the position of the objective through the optical axis isn't important for the interferogram modulation.

3.2. Decrease of the signal-to-noise ratio

A spatially incoherent illumination induces a decrease of the interferogram contrast. It is important to have a huge contrast because the interferogram is digitalized and noisy (shot-noise and electronic-noise). In the particular case of QWLSI, the phase information is obtained by demodulating the interferogram along x and y. As an incoherent illumination induces a contrast modulation along x and y of $M(KR)$ (13), the signal-to-noise ratio diminution, $SNR_{relative}$, can be described with the relation (15), plotted on the figure 5.

$$SNR_{relative}(KR) = \frac{|M(KR)|}{I_{max}/I_0} \tag{15}$$

where I_{max} is the interferogram maximum. The only possible values for I_{max} (as well as for interferogram minimum I_{min}) are given, according to equation (12), by the equation (16).

$$\frac{I_{max,min}}{I_0} \in \begin{cases} 1 + 2 \cdot M(KR) + M\left(\sqrt{2}KR\right) \\ 1 - M\left(\sqrt{2}KR\right) \\ 1 - 2 \cdot M(KR) + M\left(\sqrt{2}KR\right) \end{cases} \tag{16}$$

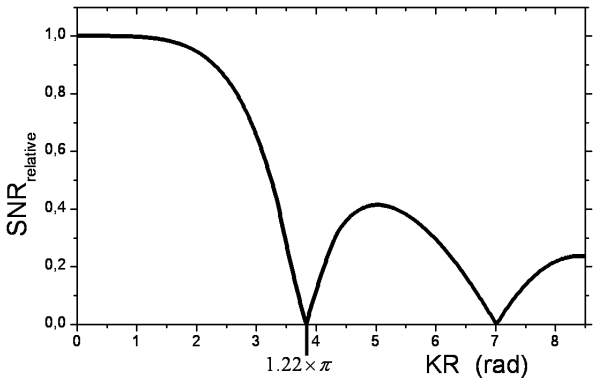

Fig. 5. Diminution of the sensitivity according to the spatial coherence of the source.

The SNR has nullification points (first one for $KR = 1.22 \cdot \pi$) : in those cases, the interferogram contrast along x and y is null and no phase-shift information can be extracted from the interferogram.

The important thing to notice here is that the SNR (as well as the interferogram contrast) only depends on the magnification of the microscope (no influence of the objective numerical

#110519 - $15.00 USD Received 24 Apr 2009; revised 3 Jul 2009; accepted 6 Jul 2009; published 16 Jul 2009

aperture) and the MHM grating. For example, with a $\times 150$ objective, a CCD-grating distance $z \approx 1500\mu m$ and a wide-opened $NA = 0.52$ condenser, the SNR decreases of about 0.7% (no visible effect on a real measurement).

3.3. Effect of spatial coherence with thick samples : OPD superposition

For phase-shift measurements, a partially coherent measurement gives results that can be difficult to interpret. Indeed, all illumination angles do not follow the same optical path within the sample. This effect is more important for larger illumination angles. Moreover, the trace of out-of-focus objects is shifted differently for each illumination angle : phase information of out-of-focus planes is spread. This effect is more important for thick samples.

In the case of a spatially incoherent source, all these illumination angles are acquired at the same time. The information carried by each angle is mixed with the others and the quantitative effect on OPD measurements under spatially incoherent illumination is not trivial, in particular with a high numerical-aperture condenser, and is beyond the scope of this paper. However, when a thin sample (like an adherent COS7 cell, part 6) is observed with a high magnification (x100), the difference between a phase measurement with a conventional wide-opened $NA = 0.52$ condenser and a phase measurement with an aperture diaphragm closed to the minimum is experimentally quite invisible.

4. Experimental setup

A commercial quadriwave lateral shearing interferometer (SID4-HR, Phasics SA, Palaiseau, France) is used here. It is an easy to integrate and compact solution (dimension of a simple camera). The SID4-HR gives 300×400 phase and intensity measurement points with a lateral pitch of $p = 29.6\mu m$. The microscope (TE-2000U, Nikon, Japan) is a conventional inverted microscope used with Nikon objectives (magnification $\times 20$, $NA = 0.5$; magnification $\times 100$, $NA = 1.3$) and a $\times 1$ or $\times 1.5$ tube lenses ; the SID4-HR is mounted on a C-mount adapter on one of the microscope's lateral camera ports and the preparation studied is imaged on the camera sensor. We work with a transmission white-light Köhler illumination. Figure 1 schematizes our configuration.

This phase and intensity lateral sampling p has to be compared with the lateral resolution of a diffraction limited microscope r. According to the Rayleigh criterion, the lateral resolution is:

$$r = \frac{0.61 \times \lambda}{NA_{obj}} \tag{17}$$

where λ is the source wavelength, NA_{obj} the object numerical aperture.

By choosing p and a camera pixel size a respecting the equation 18, with a microscope magnification g_y, the phase and intensity sampling is diffraction limited.

$$4 \cdot a = p \leq r \cdot g_y \tag{18}$$

With a SID4-HR, $p = 29.6\mu m$. By using a common $\times 100$, $NA_{obj} = 1.3$ immersion objective and $\times 1.5$ tube lens, $r = 38\mu m @ \lambda = 500nm$. In this case, the phase and intensity sampling is diffraction limited.

In the case of an aberration-free microscope, with flat wavefront illumination, the measured phase is directly the optical path difference (OPD) induced by the sample, as soon as the sample is imaged on the SID4-HR CCD. If the microscope is not perfect or if the illumination wavefront is not flat, the measured OPD is the phase-shift due to the sample plus the static phase-shift due to the microscope and illumination. A relative phase-shift measure is then possible : a reference

#110519 - $15.00 USD Received 24 Apr 2009; revised 3 Jul 2009; accepted 6 Jul 2009; published 16 Jul 2009

phase-shift measure, obtained in a tissue-free region, is subtracted to all other measurements within the sample in order to remove the static OPD. In the case of an out-of-focus imaging, the measured phase-shift is the phase-shift introduced by the sample, measured after propagation. In all cases, the acquisition speed limit is limited only by the frame rate of the CCD used (for a SID4-HR, up to $10Hz$).

5. Experimental validation

5.1. Experimental validation of the contrast modulation

In order to validate the model of the interferogram formation, a comparison between the theoretical interferogram, obtained with the formula (12), and measured interferograms with variable incident illumination aperture angles θ_i is made, by measuring the contrast of each interferogram. The chosen contrast is given by the equation (19).

$$C = \frac{max(I) - min(I)}{max(I) + min(I)} = \frac{I_{max} - I_{min}}{I_{max} + I_{min}} \tag{19}$$

where the theoretical extremum values (I_{max}, I_{min}) of I are given by the equation (16).

A $\times 20$ magnification objective, with an object numerical aperture of $NA_{obj} = 0.5$, was used combined with a condenser of $NA_{light} = 0.52$. As the condenser has a numerical aperture higher than the objective, it is sure that with a fully open aperture diaphragm, the numerical aperture of the illumination is $NA_{light} = NA_{obj} = 0.5$. The illumination numerical aperture is determined experimentally for other positions of the aperture diaphragm by measuring the illuminated surface fraction of the exit pupil.

The comparison between theoretical contrast and experimental measurements is exposed in the figure 6.

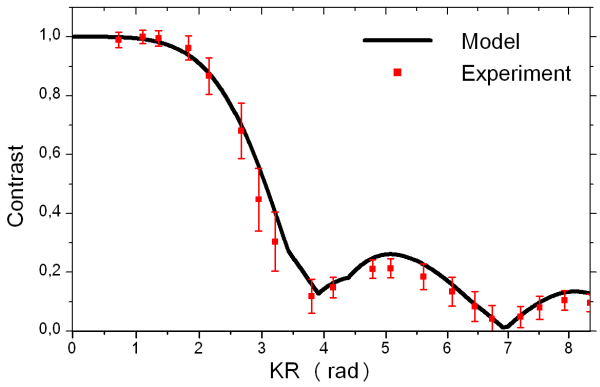

Fig. 6. Contrast comparison of simulated interferograms and acquired interferograms, for different input illumination numerical apertures. Obtained with $z = 1420\mu m$, $p = 29.6\mu m$ and $g_y = 20$.

The interferogram formation model, described by the equation (12) fits the experimental results.

For a small KR, the source tends to be spatially coherent and the contrast tends to 1. The rebounds and the angular points of the contrast function for higher KR are explained by the fact that the interferogram contrast is the combination of two Bessel functions, $M(X)$ and $M\left(\sqrt{2}X\right)$, evolving independently.

#110519 - $15.00 USD Received 24 Apr 2009; revised 3 Jul 2009; accepted 6 Jul 2009; published 16 Jul 2009

5.2. *Study of beads*

In order to verify that the measured phase-shift is directly the optical thickness along the optical axis, we first studied beads because of their modelization simplicity. We worked with polystyrene (optical index $n_{polystyrene} = 1.583 \pm 0.0005$ at $\lambda = 700nm$ [22]) spherical beads of diameter $D = 5\mu m$ into a transparent liquid of optical index $n_{liquid} = 1.552 \pm 0.0005$ at $\lambda = 700nm$ (Cargille,Cedar Grove,USA), in order to have an index step of the same order of magnitude as medium-cells. A band-pass filter $[680nn; 750nn]$ is put before the SID4-HR to reduce the refractive index wavelength dependence. The optical thickness model is very simple: a half-sphere profile with a maximum phase shift of $\varphi_{max} = D \cdot \left(n_{liquid} - n_{polystyrene}\right) = -155 \pm 4nm$. The equation 20 exposes this model in a sectioning along the center of the bead.

In this part, the studied beads can be considered to be thick compared to the microscope depth-of-field. The illumination needs to be spatially coherent in order to neglect the OPD spread effect with incoherent light (described in the part 3.3). The aperture illumination diaphragm is closed to the minimum accessible with our Köhler setup ($NA_{illumination} \approx 0.05$).

$$\delta(x) = \begin{cases} \varphi_{max} \cdot \cos\left[\arcsin\left(2 \cdot x/D\right)\right] & \text{if} \quad |x| < D/2 \\ 0 & \text{else} \end{cases} \tag{20}$$

We obtained the results shown on the figure 7 (objective $\times 100$, $NA = 1.3$; tube lens $\times 1$) :

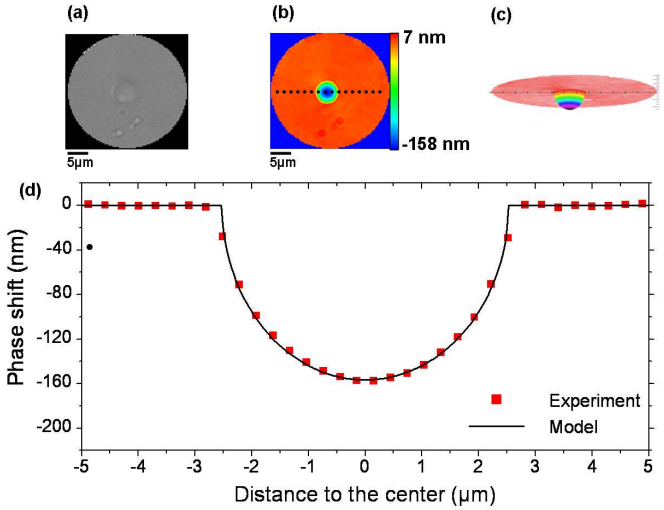

Fig. 7. (a) Intensity image of a $5\mu m$ polystyrene bead, in imaging conditions with SID4-HR, into a $n = 1.552$ transparent liquid hydrocarbon ; (b) Phase measurement (false colors) ; (c) 3D phase visualization (false colors); (d) Phase shift profile along the center of the bead, comparison between measurement and model.

The model fits very well the experiment so, in imaging conditions, wavefront sensing with SID4-HR gives a precise measurement of the optical thickness of a semi transparent sample. The maximum measured phase-shift is $\varphi = -158nm$ so δn between the bead and the medium, as D is measured at $D = 5.05\mu m$, is precisely measured at $\delta n = 0.0313 \pm 0.0001$ at $\lambda = 700nm$ and $T = 20^o$C in a single measurement.

#110519 - $15.00 USD Received 24 Apr 2009; revised 3 Jul 2009; accepted 6 Jul 2009; published 16 Jul 2009

5.3. *Study of Giant Unilamelar Vesicles*

A Giant Unilamelar Vesicle [23] (GUV) is a microscopic lipid bilayer containing a liquid solution (generally sucrose solution) surrounded by an other solution (glucose or calcium solution for example). In this study, the inside and outside solution is the same $428mmol/l$ sucrose solution : so, the refractive optical index is the same inside and outside. An incident wavefront passing through a GUV will only be phase shifted by the lipid membrane. The GUVs are made with DPPC (Dipalmitoylphosphatidylcholine).

In literature, the thickness of a DPPC lipid bilayer is given as $e = 3.85nm$ [24]. Chong and Colbow [25] measured the DPPC refractive index for some wavelengths and, using the Cauchy law from those measurements, we determined $n_{DPPC} = 1.482$ at $\lambda = 700nm$. By using the Brix index, the refractive index of the sucrose solution is $n_{medium} = 1.354$. So, theoretically, the phase-shift along the GUV center is $\varphi_{center} = 2 \cdot e \times (n_{medium} - n_{DPPC}) = -0.985nm$. The phase-shift model is the phase-shift introduced by a spherical thin membrane.

The detection of the GUV is enhanced with the phase shift visualization (figure 8). This observation was made with $\times 150$ magnification and $NA = 1.3$.

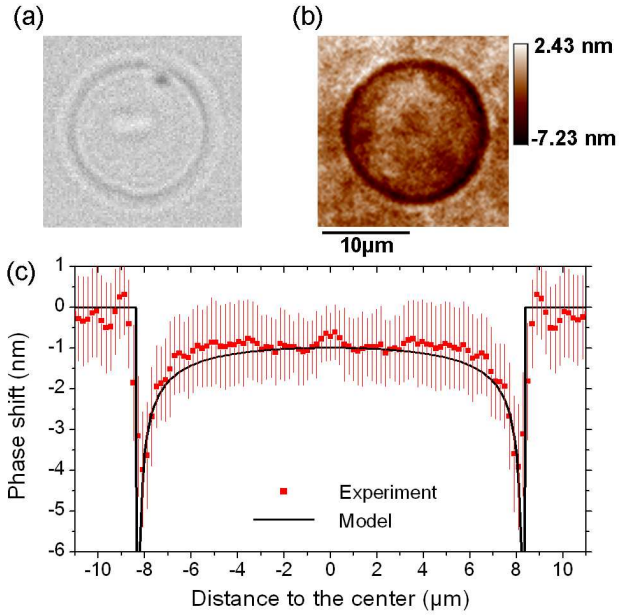

Fig. 8. (a) Intensity image, in imaging conditions, of a DPPC GUV without optical index difference between inside and outside the GUV ; (b) Phase-shift image ; (c) Phase-shift value compared to the distance from the GUV center. Red squares : Azimuthal average of the phase-shift map; the symmetry before and after $x = 0$ is explained by the complete 2π averaging. Vertical red lines : error bars, Azimuthal standard deviation. Solid black line : Theoretical phase-shift profile obtained for $D = 16.65\mu m$, $e = 3.85nm$ and $\delta n = n_{DPPC} - n_{medium} = 0.128$.

D is measured to be $16.65\mu m$ on the phase-shift image. The index difference between the membrane (DPPC) and the medium (sucrose solution) is measured by finding the best fit of the spherical thin membrane model : $\delta n = n_{DPPC} - n_{medium} = 0.11 \pm 0.04$. As the medium refractive index is $n_{medium} = 1.354$, the measured DPPC refractive index is then $n_{DPPC} = 1.46 \pm 0.04$: this measurement agrees with the theory.

#110519 - $15.00 USD Received 24 Apr 2009; revised 3 Jul 2009; accepted 6 Jul 2009; published 16 Jul 2009

The sensibility is sufficient to contrast small phase-shift measurements of a few *nm*. We demonstrate that a two layer membrane is visible directly with a SID4-HR phase-shift measurement.

6. Measurements on living cells (COS-7)

COS-7 [26] are mutant green monkey kidney cells, adherent on their substrate. This kind of cell is interesting for studying membrane dynamics and intracellular movements [27] because of its small thickness. The geometry of such a cell is variable, with important shape modifications (ruffles, lamellipodium growth). The intensity contrast is very low and phase shift measurements allow a real enhancement of this contrast as presented in the Fig. 9 (Media 1), (Media 2) (magnification $\times 150$, $NA = 1.3$).

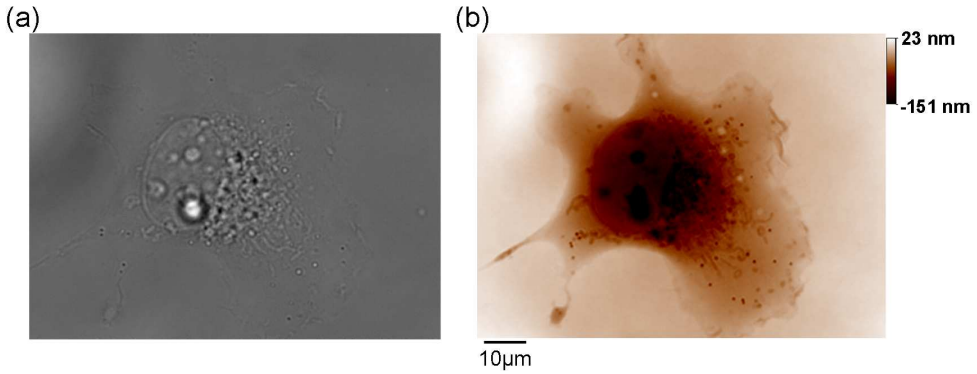

Fig. 9. Single frame excerpts from (Media 1), (Media 2). (a) Intensity image, in imaging conditions, of COS-7 cells ; (b) Phase image.

The influence of the nucleus is clearly visible in the image center and a precise visualization and tracking of vesicles is possible. Ruffles on the membrane can also be observed in the cell periphery. The phase-shift sensibility is huge (OPD noise of less than $1nm$) and very small phase-shift are visible, in particular on the lamellipodia arround the cell.

The quantification of phase shift permits, with a hypothesis about the thickness, a direct determination of the refractive index of the elements constituting the cell. But, for now, the precise identification of each phase-contrasted cell constituents is not complete and the refractive index listing is in progress.

7. Conclusions and perspectives

In this paper, the interests for microscopy of high-resolution wavefront sensing by QWLSI have been demonstrated : a lateral resolution up to the microscope diffraction limit with 300×400 images, a huge OPD sensitivity of less than $1nm$ and the implementation simplicity. Indeed, this technique does not require temporally coherent illumination, so it can be used with conventional microscope sources, such as halogen lamps. Furthermore, since the interferogram formation does not depend on the wavelength, broadband sources are suitable for illumination. Therefore, no modification is needed to use QWLSI on a conventional bright-field microscope. Moreover, this makes it not only compatible but also complementary with other imaging techniques such as fluorescence or non-linear techniques.

We studied the influence of the illumination spatial coherence. We concluded that if a low-noise quantitative measurement of the phase-shift is needed, the illumination spatial coherence

#110519 - $15.00 USD Received 24 Apr 2009; revised 3 Jul 2009; accepted 6 Jul 2009; published 16 Jul 2009

should be carefully controlled, with a Köhler set-up for instance. For thick samples, we showed that the phase information could be altered when the illumination coherence is too low, mostly because the source points have different optical paths. This effect will be studied further and is negligible when the spatial coherence increases. In the particular case of thin samples, observed with high magnification, the illumination spatial coherence is not critical.

The study of easily modeled samples confirmed the acuity and sensitivity of OPD measurements in imaging conditions. The interest for visualizing OPD becomes particularly interesting when biological phase-only microscopic samples are observed.

At least two classes of applications are envisioned : phase contrast images and quantitative index reconstruction. Mapping the OPD gives more information on the samples. Image processing on this quantitative information is possible and useful for particle tracking and small phase-shift enhancement.

#110519 - $15.00 USD Received 24 Apr 2009; revised 3 Jul 2009; accepted 6 Jul 2009; published 16 Jul 2009